

Spatio-Temporal Data Fusion for Massive Sea Surface Temperature Data from MODIS and AMSR-E Instruments

Pulong Ma

Statistical and Applied Mathematical Sciences Institute
and Duke University

79 T.W. Alexander Drive, P.O. Box 110207

Durham, NC 27709

Emily L. Kang

Department of Mathematical Sciences, University of Cincinnati
Cincinnati, OH 45220

Abstract

Remote sensing data have been widely used to study many geophysical processes. With the advance of remote-sensing technology, massive amount of remote sensing data are collected in space over time. Different satellite instruments typically have different footprints, measurement-error characteristics, and data coverage. To combine datasets from different instruments, we propose a dynamic fused Gaussian process (DFGP) model that enables fast statistical inference such as smoothing and filtering for massive spatio-temporal datasets in the data-fusion context. Based upon the spatio-temporal-random-effects model, the DFGP methodology represents the underlying true process with two components: a linear combination of a small number of basis functions and random coefficients with a general covariance matrix and a linear combination of a large number of basis functions and Markov random coefficients. To model the true process at different spatial resolutions, we rely on the change-of-support property, since it allows efficient computations in DFGP. To estimate model parameters, we devise a computationally efficient stochastic expectation-maximization (SEM) algorithm to ensure its scalability for massive datasets. The DFGP model is applied to a total of 3.7 million sea surface temperature datasets in a one-week period in tropical Pacific Ocean area from MODIS and AMSR-E instruments.

Keywords: Dynamic fused Gaussian process; Spatio-temporal data fusion; Basis functions; Change of support; Massive datasets; Sea surface temperature

1 Introduction

Remote sensing technology has been advancing the measurement of massive amount of datasets for many geophysical processes. Statistical analysis for massive amount of data is challenging, since many geophysical processes evolves in space and time with complicated structures. The resulting data often exhibit nonstationary dependence structures. As remote sensing data are often collected by different satellite instruments over different footprints with distinct shapes, orientations, and sizes, these remote-sensing data are often noisy and incomplete with incompatible spatial supports and distinct measurement-error characteristics.

To analyze data from different satellite instruments, the resolution difference must be accounted for. There is a vast literature in spatial statistics to tackle the so-called change-of-support problem when statistical analysis is carried out with several data sources at different resolutions. Here, change of support (COS) refers to inference made at a resolution based on data from different scales (e.g., Cressie, 1993, 1996; Gelfand et al., 2001; Gotway and Young, 2002). A direct way to deal with the change-of-support problem is to represent the process at the block level as a stochastic integral of the process at the point level or areal-unit level. When data are obtained at different scales or resolutions, statistical inference for combining such data leads to the data-fusion problem. In spatial-statistics literature, data fusion has been approached in several different ways. Wikle and Berliner (2005) formulate a hierarchical Bayesian model that combines observations across different scales by assuming the same underlying true process. In a similar way, Fuentes and Raftery (2005) present an instance of Bayesian melding (Poole and Raftery, 2000) that assumes the underlying true process at the point level so that point-referenced observations of air pollution data and air-quality model output at the grid-cell level are linked to a same true process at the point level via measurement-error processes. The space-time extension of Fuentes and Raftery (2005) has been developed in Choi et al. (2009) to study the spatio-temporal association between mortality and pollution exposure to daily fine particulate matter ($PM_{2.5}$) based on point-referenced $PM_{2.5}$ and an air quality model output. These models address the change-of-support problem explicitly, but their implementations require expensive computations, and hence their models are not suitable to handle large datasets. Other different approaches for data fusion have been developed as well. For instance, McMillan et al. (2010) present a spatio-temporal model that combines point-referenced observations and numerical model outputs at the grid-cell level by assuming that the data pro-

cess are linked to the same underlying true process at the grid-cell level instead of at the point level. Instead of assuming the same true underlying process for both observations and numerical model output, Berrocal et al. (2010, 2012) propose to regress the point-referenced observations over model output at the grid-cell level with spatial or spatio-temporal varying coefficients. These models have been applied to make inference based on point-referenced air quality observations and numerical model outputs at grid-cell level over the United States. In a similar way, Sahu et al. (2010) also regress the point-referenced true process over numerical model outputs at the grid-cell level to predict chemical deposition in eastern United States. These approaches do not address the change-of-support explicitly, and they require intensive computations to fit the model in a Bayesian framework. In remote sensing science, massive amount of data are often collected over space and time by satellite instruments, making these methods computationally intractable.

To tackle the massiveness of remote-sensing data, Nguyen et al. (2012) present the spatial data fusion methodology based on the spatial-random-effects model (Cressie and Johannesson, 2006, 2008), where a single underlying true spatial process is assumed at the areal-unit level. Nguyen et al. (2014) further develop the spatio-temporal data fusion methodology based on the spatio-temporal-random-effects model (Cressie et al., 2010; Kang et al., 2010; Katzfuss and Cressie, 2011, 2012), where different underlying true spatio-temporal processes are assumed at the areal-unit level, and cross-dependence structures among different true processes are modeled through the spatio-temporal-random-effects model.

In this article, we propose a dynamic fused Gaussian process (DFGP) methodology for spatio-temporal data fusion to combine multiple datasets from different satellite instruments. As a generalization of Nguyen et al. (2014), our DFGP methodology extends the spatial-only fused Gaussian process (FGP) in Ma and Kang (2018) to a spatio-temporal setting. In particular, the FGP model extends the fixed rank kriging (FRK) model (Cressie and Johannesson, 2006, 2008) by combining a low-rank representation with a general covariance matrix and a graphical model with a sparse precision matrix. Based upon FGP, we take a dynamic-statistical approach to build the DFGP model under which current state of the process of interest evolves from previous state in a dynamic way. This hierarchical modeling approach has been adopted in many previous research (e.g., Mardia et al., 1998; Wikle et al., 1998; Wikle and Cressie, 1999; Berliner et al., 2000; Stroud et al., 2001; Wikle et al., 2001; Huang et al., 2002; Cressie and Wikle, 2002; Xu and Wikle, 2007);

see Cressie and Wikle (2011) for a comprehensive overview for spatio-temporal models. Our proposed DFGP falls into this paradigm, and extends the spatio-temporal-random-effects model (Cressie et al., 2010; Kang et al., 2010; Katzfuss and Cressie, 2011, 2012) with a more flexible covariance function.

This article is organized as follows. Section 2 introduces two different datasets from two satellite instruments onboard NASA’s Aqua satellite. Section 3 presents the dynamic fused Gaussian process methodology in the data fusion context. Kalman filtering and Kalman smoothing procedures are also derived. In Section 4, we give details on the stochastic expectation-maximization algorithm for parameter estimation in both filtering and smoothing procedures. In Section 5, we apply the DFGP methodology to analyze massive amount of sea surface temperature datasets, and make comparisons with other existing methods such as the spatio-temporal data fusion model in Nguyen et al. (2014). Section 6 concludes with remarks and future research work.

2 Data

Sea surface temperature (SST) is a key climate and weather measurement, which plays a crucial role in understanding climate systems. Massive amount of SST datasets can be collected from satellite instruments each day with the advance of new remote-sensing technologies. For instance, the AQUA satellite launched on May 4, 2002 is a polar-orbiting satellite around the Earth, aiming at studying Earth’s precipitation, evaporation, and cycling of water. The AQUA satellite carries two instruments: the Moderate Resolution Imaging Spectroradiometer (MODIS) and the Advanced Microwave Scanning Radiometer-Earth Observing System (AMSR-E). The MODIS instrument is an infrared radiometer with a ground swath width of 2,330 km, which is able to measure SST at fine spatial resolutions, but unable to measure through cloud cover; the AMSR-E instrument is a microwave radiometer with a ground swath width of 1445 km, which is able to measure SST in all weather conditions except rain, but only at coarse spatial resolutions, and its quality is also subject to radio frequency interference. Although MODIS SST and AMSR-E SST data have been widely used for scientific research and operations (e.g., Donlon et al., 2002; O’Carroll et al., 2006; Gentemann, 2014), *ad hoc* combination of these two different data products can be problematic in practice due to their different error characteristics and incompatible supports. In addition, high-

resolution SST products are often required for operational oceanography and numerical weather prediction. Their generation should be based on several different remote-sensing satellites and calibrated by direct measurements such as in-situ observations (e.g., Guan and Kawamura, 2003; Kawai et al., 2006; Arai, 2013). In this article, we generate such high-resolution SST data products on a daily scale by combining MODIS SST and AMSR-E SST data in a statistical rigorous way.

In this study, we use daily daytime MODIS SST data at 9 km spatial resolution processed from the NASA Ocean Biology Processing Group Data Center (oceancolor.gsfc.nasa.gov), and daily daytime AMSR-E SST data at 25 km spatial resolution from www.remss.com in the year 2010. These data have distinct error characteristics and are often sparse, irregular, and noisy with incompatible supports. Statistical methods for combining different sources of remote-sensing data will give much more accurate and reliable uncertainty analysis. The study region is chosen to be the tropical Pacific region between longitude -30° and 30° and between latitude 120° and 290° from January 1 to 8 in the year 2010. Figure 1 shows the MODIS SST and AMSR-E SST on January 1, 2010. The number of observations from MODIS instrument for each day are $n_1^{(1)} = 362,721, n_2^{(1)} = 398,662, n_3^{(1)} = 409,445, n_4^{(1)} = 385,490, n_5^{(1)} = 425,541, n_6^{(1)} = 415,869, n_7^{(1)} = 416,721, n_8^{(1)} = 415,467$, resulting in a total of 3,229,916 MODIS SST observations, where the subscript denotes the time step, and superscript denotes the instrument with 1 for MODIS and 2 for AMSR-E. The number of observations from AMSR-E instrument for each day are $n_1^{(2)} = 71,592, n_2^{(2)} = 68,574, n_3^{(2)} = 72,905, n_4^{(2)} = 64,868, n_5^{(2)} = 73,228, n_6^{(2)} = 66778, n_7^{(2)} = 71,431, n_8^{(2)} = 67,245$, resulting in a total of 556,621 AMSR-E SST observations.

3 Dynamic Fused Gaussian Process

For many physical spatio-temporal processes, it's quite natural that the process of interest cannot be observed directly, and we assume that the observed data is a sum of the hidden process and measurement noise. Suppose we are interested in a real-valued spatio-temporal process $\{Y_t(\mathbf{s}) : \mathbf{s} \in \mathcal{D} \subset \mathbb{R}^d, t \in \mathcal{T}\}$, where $\mathcal{D} \subset \mathbb{R}^d$ and $\mathcal{T} \equiv \{1, 2, \dots, T\}$ for positive integer T . The goal is to make fast statistical inference such as filtering and smoothing based on massive spatio-temporal datasets. What follows is to define the dynamic fused Gaussian process (DFGP) model.

Suppose that the spatial domain \mathcal{D} of interest is made up of N non-overlapping, basic areal

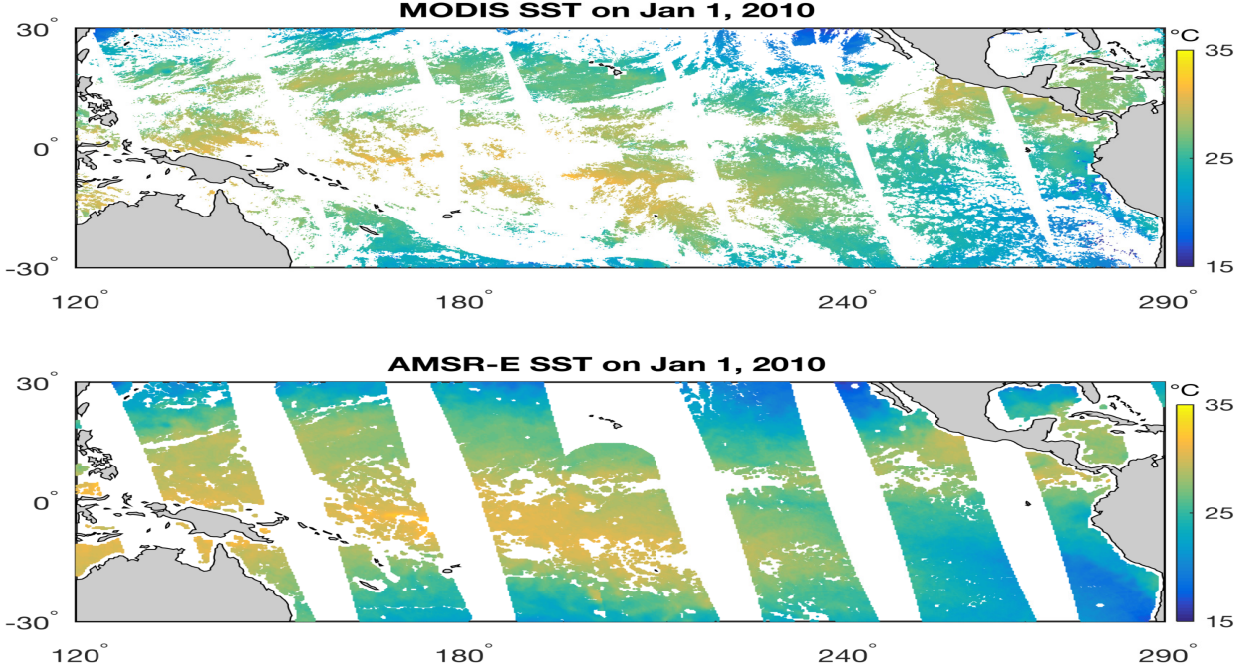


Figure 1. MODIS and AMSR-E SST data on January 1, 2010. The MODIS SST data are at 9 km resolution and the AMSR-E SST data are at 25 km resolution.

units \mathcal{R}_i associated with centroid s_i for $i = 1, \dots, N$. These basic areal units represent the smallest spatial resolution at which prediction will be made, and they are called BAUs. This discretization procedure has been used in many previous work (e.g., Cressie and Johannesson, 2006, 2008; Nguyen et al., 2012, 2014; Shi and Kang, 2017; Ma and Kang, 2018; Ma et al., 2018). The data process is assumed to be observed at different spatial resolutions resulting from the same underlying true process $Y_t(\cdot)$ over these BAUs. This is a typical situation where multiple satellite instruments measure the same geophysical process at different resolutions in remote-sensing science. Let $\mathbf{Z}_t^{(k)} \equiv (Z_t(\mathcal{A}_{1,t}^{(k)}), \dots, Z_t(\mathcal{A}_{n_t^{(k)},t}^{(k)}))'$ be a vector of noisy version of the underlying true process $Y_t(\cdot)$ at k -th resolution over $n_t^{(k)}$ footprints $\{\mathcal{A}_{t,i}^{(k)} : i = 1, \dots, n_t^{(k)}\}$ from the k -th satellite instrument at time t , where the quantity with superscript k corresponds to that from k -th satellite instrument. The total number of observations at time t is denoted as $n_t = \sum_{k=1}^{k_0} n_t^{(k)}$ across all resolutions. The observed value $Z_t(\cdot)$ over the i -th footprint $\mathcal{A}_{t,i}^{(k)}$ from k -th instrument at time t is modeled as the true process $Y(\cdot)$ over footprint $\mathcal{A}_{t,i}^{(k)}$ plus a measurement-error process:

$$Z_t(\mathcal{A}_{t,i}^{(k)}) = Y_t(\mathcal{A}_{t,i}^{(k)}) + \epsilon_t(\mathcal{A}_{t,i}^{(k)}), \quad \mathcal{A}_{t,i}^{(k)} \subset \mathcal{D}; i = 1, \dots, n_t^{(k)}; k = 1, \dots, k_0 \quad (3.1)$$

The true process $Y_t(\cdot)$ over the footprint $\mathcal{A}_{t,i}^{(k)}$ is assumed to be the block average of the process $Y_t(\cdot)$ over the BAUs within the domain $\mathcal{A}_{t,i}^{(k)}$:

$$Y_t(\mathcal{A}_{t,i}^{(k)}) = \frac{1}{\sum_{\mathbf{s} \in \mathcal{D}} I(\mathbf{s} \in \mathcal{A}_{t,i}^{(k)})} \sum_{\mathbf{s} \in \mathcal{D}} I(\mathbf{s} \in \mathcal{A}_{t,i}^{(k)}) \cdot Y(\mathbf{s}). \quad (3.2)$$

where the Eq. (3.2) is accounting for the change-of-support problem. Another way to address the change-of-support problem is to define the process at coarse resolution to be a stochastic integral of the process at fine resolution: $Y_t(\mathcal{A}_{t,i}^{(k)}) = \frac{1}{|\mathcal{A}_{t,i}^{(k)} \cap \mathcal{D}|} \int_{\mathcal{A}_{t,i}^{(k)}} Y(\mathbf{s}) d\mathbf{s}$. To compute this integral, one has to use its discretized version such as Eq. (3.2) in practice. This strategy has been widely taken in previous work (e.g., Wikle et al., 2001; Gelfand et al., 2001; Nguyen et al., 2012, 2014, 2017; Katzfuss and Cressie, 2011, 2012; Nguyen et al., 2017; Ma et al., 2018; Fuentes and Raftery, 2005).

The measurement-error process $\epsilon_t(\cdot)$ is assumed to be spatially independent. It may have nonzero mean capturing the instrument bias, and has variance $\text{var}(\epsilon_t(\mathcal{A}_{t,i}^{(k)})) = \sigma_{\epsilon_t, (k)}^2 v(\mathcal{A}_{t,i}^{(k)}) > 0$; where $v(\mathcal{A}_{t,i}^{(k)})$ is known from validation data and instrument specification and allows for the possibility of nonconstant variance over the domain \mathcal{D} . The variance parameter $\sigma_{\epsilon_t, (k)}^2$ will be estimated via a maximum likelihood estimation procedure in Section 4. Under this assumption, the nugget variance parameters are both instrument-dependent and time-dependent. This allows great flexibility in modeling the measurement-error processes. The data model defined by Eq. (3.1) and (3.2) has been studied in many previous work (e.g., Nguyen et al., 2012, 2014).

As we are interested in the process $Y_t(\cdot)$ at finest resolution defined by N BAUs. Following Fuentes and Raftery (2005); Nguyen et al. (2012, 2014); Ma et al. (2018), we define the process of interest $\{Y_t(\mathbf{s}) : \mathbf{s} \in \mathcal{D}\}$ at BAU levels:

$$\text{Process model 1: } Y_t(\mathbf{s}) = \mathbf{X}_t(\mathbf{s})' \boldsymbol{\beta}_t + \nu_t(\mathbf{s}) + \delta_t(\mathbf{s}), \quad (3.3)$$

$$\text{Process model 2: } \nu_t(\mathbf{s}) = \mathbf{S}_t(\mathbf{s})' \boldsymbol{\eta}_t, \quad (3.4)$$

$$\text{Process model 3: } \delta_t(\mathbf{s}) = \mathbf{B}_t(\mathbf{s})' \boldsymbol{\xi}_t, \quad (3.5)$$

where $\mathbf{X}_t(\cdot) \equiv (X_{t,1}(\cdot), \dots, X_{t,p}(\cdot))'$ is a p -dimensional vector of covariates and $\boldsymbol{\beta}_t$ are corre-

sponding unknown coefficients at time t ; $\mathbf{S}_t(\cdot) \equiv (S_{t,1}(\cdot), \dots, S_{t,r}(\cdot))'$ is an r -dimensional vector of basis functions at time t , and $\boldsymbol{\eta}_t$ is an r -dimensional random vector. Following Cressie and Johannesson (2008), we choose a bisquare basis function with the following form: $S_{t,i}(\mathbf{u}) = \{1 - (\|\mathbf{u} - \mathbf{c}_i\|/\ell_i)^2\}^2 \cdot \{I(\|\mathbf{u} - \mathbf{c}_i\| \leq \ell_i)\}$ for $i = 1, \dots, r$, where \mathbf{c}_i is the center of the i -th bisquare basis function, and ℓ_i is the corresponding radius of the i -th bisquare basis function. In addition, we also assume that the number of basis functions is much smaller than the number of observations, i.e., $r \ll n_t$. The model in Eq (3.4) has a low-rank representation. $\mathbf{B}_t(\cdot) \equiv (B_{t,1}(\cdot), \dots, B_{t,N}(\cdot))'$ is an N -dimensional vector of basis functions for the Markov random coefficients $\boldsymbol{\xi}_t$ at time t . $\boldsymbol{\xi}_t$ is a N -dimensional random vector defined on N BAUs with Markov structure specified in Eq. (3.7). Following Ma and Kang (2018), we choose a piecewise linear basis function for $B_{t,i}(\cdot)$ with the following form: $\mathbf{B}_{t,i}(\mathbf{u}) = I(\mathbf{u} \in \mathcal{R}_i)$ for $i = 1, \dots, N$. The model in Eq. (3.5) has a high-rank representation, since $N \approx n_t$ or $N > n_t$. Notice that the quantities $\mathbf{X}_t(\cdot)$, $\mathbf{S}_t(\cdot)$, $\mathbf{B}_t(\cdot)$ are defined at BAU-level, resulting in a model for the underlying true process $Y_t(\cdot)$ also at BAU-level. However, the actually observation is defined at a resolution that is coarser than the resolution at which these BAUs are defined. The Eq. (3.2) links the process $Y_t(\cdot)$ at BAU-level to the resolution at which the data process is defined through the change-of-support property. In what follow, we will give the model specification for $\boldsymbol{\eta}_t$ and $\boldsymbol{\xi}_t$.

Following Cressie et al. (2010), we assume that the dynamical evolution of $\{\boldsymbol{\eta}_t : t = 0, 1, \dots, T\}$ follows a vector-autoregressive (VAR) model :

$$\boldsymbol{\eta}_t \mid \boldsymbol{\eta}_{t-1}, \boldsymbol{\eta}_{t-2}, \dots, \boldsymbol{\eta}_0 \sim \mathcal{N}_r(\mathbf{H}_t \boldsymbol{\eta}_{t-1}, \mathbf{U}_t), \quad t = 1, 2, \dots, T, \quad (3.6)$$

with initial state $\boldsymbol{\eta}_0 \sim \mathcal{N}_r(\mathbf{0}, \mathbf{K}_0)$. The $r \times r$ matrix \mathbf{H}_t and $r \times r$ matrix \mathbf{U}_t are referred to as the propagation matrix and innovation covariance matrix, respectively.

The spatial-temporal process $\delta_t(\cdot)$ is linked to the random vector $\boldsymbol{\xi}_t$ through the link matrix $\mathbf{B}_t(\cdot)$. Consider pairwise disjoint subregions $\{\mathcal{R}_i : i = 1, \dots, N\}$, which partition the spatial domain \mathcal{D} , and define $\boldsymbol{\xi}_t = (\xi_t(\mathcal{R}_1), \dots, \xi_t(\mathcal{R}_N))'$ for $t = 1, \dots, T$. We assume the following parsimonious spatial-temporal model for $\boldsymbol{\xi}_t$: for $i = 1, \dots, N$,

$$\xi_t(\mathcal{R}_i) \mid \boldsymbol{\xi}_t^{-i} \sim \mathcal{N}(\gamma_t/e_{i+} \cdot \sum_{j \in \partial \mathcal{R}} e_{ij} \xi_t(\mathcal{R}_j), \tau_t^2/e_{i+}), \quad (3.7)$$

where $\boldsymbol{\xi}_t^{-i} \equiv (\xi_t(\mathcal{R}_1), \dots, \xi_t(\mathcal{R}_{i-1}), \xi_t(\mathcal{R}_{i+1}), \dots, \xi_t(\mathcal{R}_N))'$; $\mathbf{E} = (e_{ij})$ is an $N \times N$ adjacency

matrix on discretized domain $\mathcal{D} = \cup_{i=1}^N \mathcal{R}_i$; γ_t is the spatial dependence parameter at time t , and ρ_t is the temporal dependence parameter at time t ; and $e_{i+} = \sum_{j=1}^N e_{ij}$. From Eq. (3.7), it is easy to derive that the joint conditional distribution of $\boldsymbol{\xi}_t$ for $t = 1, \dots, T$, is

$$\boldsymbol{\xi}_t \sim \mathcal{N}(\mathbf{0}, \mathbf{Q}_t^{-1}), \quad (3.8)$$

where $\mathbf{Q}_t \equiv \boldsymbol{\Delta}^{-1}(\mathbf{I} - \gamma_t \mathbf{W})/\tau_t^2$; $\mathbf{W} \equiv \boldsymbol{\Delta} \cdot \mathbf{E}$ is the $N \times N$ proximity matrix, and $\boldsymbol{\Delta} \equiv \text{diag}(1/e_1, \dots, 1/e_N)$. This model is a conditional autoregressive (CAR) model. The model for $\delta_t(\cdot)$ is hence called a Gaussian graphical model (GGM). As discussed in Ma and Kang (2018), the model for $\delta_t(\cdot)$ can be constructed in a similar way as in Lindgren et al. (2011) and Nychka et al. (2015). This will increase the flexibility of the model. Such implementation and demonstration is beyond the scope of this article. Although the model for $\delta_t(\cdot)$ is currently assumed to be temporally independent, the temporal evolution is described by the random vectors $\{\boldsymbol{\eta}_t : t = 1, \dots, T\}$.

Define the following quantities:

$$X_{t,i}(\mathcal{A}_{t,j}^{(k)}) \equiv \frac{1}{\sum_{\mathbf{s} \in \mathcal{D}} I(\mathbf{s} \in \mathcal{A}_{t,j}^{(k)})} \sum_{\mathbf{s} \in \mathcal{D}} I(\mathbf{s} \in \mathcal{A}_{t,j}^{(k)}) \cdot X_{t,i}(\mathbf{s}), \quad i = 1, \dots, p, \quad (3.9)$$

$$S_{t,i}(\mathcal{A}_{t,j}^{(k)}) \equiv \frac{1}{\sum_{\mathbf{s} \in \mathcal{D}} I(\mathbf{s} \in \mathcal{A}_{t,j}^{(k)})} \sum_{\mathbf{s} \in \mathcal{D}} I(\mathbf{s} \in \mathcal{A}_{t,j}^{(k)}) \cdot S_{t,i}(\mathbf{s}), \quad i = 1, \dots, r, \quad (3.10)$$

$$B_{t,i}(\mathcal{A}_{t,j}^{(k)}) \equiv \frac{1}{\sum_{\mathbf{s} \in \mathcal{D}} I(\mathbf{s} \in \mathcal{A}_{t,j}^{(k)})} \sum_{\mathbf{s} \in \mathcal{D}} I(\mathbf{s} \in \mathcal{A}_{t,j}^{(k)}) \cdot B_{t,i}(\mathbf{s}), \quad i = 1, \dots, N, \quad (3.11)$$

where $t = 1, \dots, T$; $k = 1, \dots, k_0$; $j = 1, \dots, n_t^{(k)}$. By combining Eq (3.1) through Eq (3.5), we have the following general linear model at k -th resolution:

$$Z_t(\mathcal{A}_{t,i}^{(k)}) = \mathbf{X}_t(\mathcal{A}_{t,i}^{(k)})' \boldsymbol{\beta}_t + \mathbf{S}_t(\mathcal{A}_{t,i}^{(k)})' \boldsymbol{\eta}_t + \mathbf{B}_t(\mathcal{A}_{t,i}^{(k)})' \boldsymbol{\xi}_t + \boldsymbol{\epsilon}_t(\mathcal{A}_{t,i}^{(k)}). \quad (3.12)$$

Now stacking the above model over all footprints from k -th instrument at time t yields the following representation:

$$\mathbf{Z}_t^{(k)} = \mathbf{X}_t^{(k)} \boldsymbol{\beta}_t + \mathbf{S}_t^{(k)} \boldsymbol{\eta}_t + \mathbf{B}_t^{(k)} \boldsymbol{\xi}_t + \boldsymbol{\epsilon}_t^{(k)}, \quad k = 1, \dots, k_0, \quad (3.13)$$

where $\mathbf{X}_t^{(k)} \equiv [\mathbf{X}_t(\mathcal{A}_{t,1}^{(k)}), \dots, \mathbf{X}_t(\mathcal{A}_{t,n_t^{(k)}}^{(k)})]'$ is an $n_t^{(k)}$ -by- p matrix. $\mathbf{S}_t^{(k)} \equiv [\mathbf{S}_t(\mathcal{A}_{t,1}^{(k)}), \dots, \mathbf{S}_t(\mathcal{A}_{t,n_t^{(k)}}^{(k)})]'$ is an $n_t^{(k)}$ -by- r basis matrix in the low-rank component. $\mathbf{B}_t^{(k)} \equiv [\mathbf{B}_t(\mathcal{A}_{t,1}^{(k)}), \dots, \mathbf{B}_t(\mathcal{A}_{t,n_t^{(k)}}^{(k)})]'$ is an $n_t^{(k)}$ -by- N basis matrix in the GGM component. $\boldsymbol{\epsilon}_t^{(k)} \equiv [\boldsymbol{\epsilon}_t(\mathcal{A}_{t,1}^{(k)}), \dots, \boldsymbol{\epsilon}_t(\mathcal{A}_{t,n_t^{(k)}}^{(k)})]'$ is an $n_t^{(k)}$ -dimensional random vector whose covariance matrix is $\sigma_\epsilon^2 \mathbf{V}_{\epsilon_t, (k)}$ with $\mathbf{V}_{\epsilon_t, (k)} \equiv \text{diag}\{v(\mathcal{A}_{t,1}^{(k)}), \dots,$

$v(\mathcal{A}_{t,n_t}^{(k)})\}$.

Let $\mathbf{Z}_t \equiv [\mathbf{Z}_t^{(1)'}, \dots, \mathbf{Z}_t^{(k_0)'}]'$ denote an n_t -dimensional vector stacking all the observations together from k_0 satellite instruments at time t . Let $\mathbf{X}_t \equiv [\mathbf{X}_t^{(1)'}, \dots, \mathbf{X}_t^{(k_0)'}]'$ denote an n_t -by- p matrix stacking all the covariates corresponding to all the observations at time t . Let $\mathbf{S}_t \equiv [\mathbf{S}_t^{(1)'}, \dots, \mathbf{S}_t^{(k_0)'}]'$ be an n_t -by- r basis matrix in the low-rank component. Let $\mathbf{B}_t \equiv [\mathbf{B}_t^{(1)'}, \dots, \mathbf{B}_t^{(k_0)'}]'$ be an n_t -by- N basis matrix in the GGM component. Then we have

$$\mathbf{Z}_t = \mathbf{X}_t \boldsymbol{\beta}_t + \mathbf{S}_t \boldsymbol{\eta}_t + \mathbf{B}_t \boldsymbol{\xi}_t + \boldsymbol{\epsilon}_t, \quad (3.14)$$

where $\boldsymbol{\epsilon}_t \equiv (\boldsymbol{\epsilon}_t^{(1)'}, \dots, \boldsymbol{\epsilon}_t^{(k_0)'})'$ is an n_t -dimensional random vector with covariance matrix $\mathbf{V}_t \equiv \text{diag}\{\sigma_{\boldsymbol{\epsilon}_t, (1)}^2 \mathbf{V}_{\boldsymbol{\epsilon}_t, (1)}, \dots, \sigma_{\boldsymbol{\epsilon}_t, (k_0)}^2 \mathbf{V}_{\boldsymbol{\epsilon}_t, (k_0)}\}$.

3.1 Kalman Filter and Kalman Smoother

Suppose that inference is made on $Y_t(\mathbf{s}_0)$ for any spatial location $\mathbf{s}_0 \in \mathcal{D}$ and any time $t = 1, \dots, T$. Let the set \mathcal{D}^P be a collection of m_t spatial locations where we want to make prediction of $Y_t(\cdot)$ at time t . So, the process vector of interest is

$$\mathbf{Y}_t^P \equiv \mathbf{X}_t^P \boldsymbol{\beta}_t + \mathbf{S}_t^P \boldsymbol{\eta}_t + \boldsymbol{\delta}_t^P, \quad t = 1, \dots, T, \quad (3.15)$$

where superscript P denotes the quantities evaluated at the set \mathcal{D}^P of prediction locations.

In what follows, sequential updates based on the hierarchical dynamical spatio-temporal process DFGP will be derived. Let $\mathbf{Z}_{1:u} \equiv [\mathbf{Z}_1', \dots, \mathbf{Z}_u']'$. For conditional expectations of $\boldsymbol{\eta}_t$ and $\boldsymbol{\delta}_t^P$ based on $\mathbf{Z}_{1:u}$, the following notations will be used: $\boldsymbol{\eta}_{t|u} \equiv E(\boldsymbol{\eta}_t \mid \mathbf{Z}_{1:u})$ and $\boldsymbol{\delta}_{t|u}^P \equiv E(\boldsymbol{\delta}_t^P \mid \mathbf{Z}_{1:u})$. The corresponding conditional covariance matrices will be denoted as $\mathbf{P}_{t|u} \equiv \text{var}(\boldsymbol{\eta}_t \mid \mathbf{Z}_{1:u})$ and $\mathbf{R}_{1:u}^P \equiv \text{var}(\boldsymbol{\delta}_t^P \mid \mathbf{Z}_{1:u})$, respectively.

Assuming initial states $\boldsymbol{\eta}_{0|0} \equiv \mathbf{0}$ and $\mathbf{P}_{0|0} \equiv \mathbf{K}_0$, we obtain the one-step ahead forecasts:

$$\boldsymbol{\eta}_{t|t-1} = \mathbf{H}_t \boldsymbol{\eta}_{t-1|t-1} \quad (3.16)$$

$$\mathbf{P}_{t|t-1} = \mathbf{H}_t \mathbf{P}_{t-1|t-1} \mathbf{H}_t' + \mathbf{U}_t. \quad (3.17)$$

The filtering algorithm is proceeded sequentially for $t = 1, \dots, T$:

$$\boldsymbol{\eta}_{t|t} = \boldsymbol{\eta}_{t|t-1} + \mathbf{G}_t(\mathbf{Z}_t - \mathbf{X}_t\boldsymbol{\beta}_t - \mathbf{S}_t\boldsymbol{\eta}_{t|t-1}) \quad (3.18)$$

$$\mathbf{P}_{t|t} = \mathbf{P}_{t|t-1} - \mathbf{G}_t\mathbf{S}_t\mathbf{P}_{t|t-1} \quad (3.19)$$

$$\boldsymbol{\delta}_{t|t}^P = \mathbf{B}_t^P\mathbf{Q}_t^{-1}\mathbf{B}_t'[\mathbf{S}_t\mathbf{P}_{t|t-1}\mathbf{S}_t' + \mathbf{D}_t^{-1}]^{-1}(\mathbf{Z}_t - \mathbf{X}_t\boldsymbol{\beta}_t - \mathbf{S}_t\boldsymbol{\eta}_{t|t-1}) \quad (3.20)$$

$$\mathbf{R}_{t|t}^P = \mathbf{B}_t^P\mathbf{Q}_t^{-1}\mathbf{B}_t^{P'} - \mathbf{B}_t^P\mathbf{Q}_t^{-1}\mathbf{B}_t'[\mathbf{S}_t\mathbf{P}_{t|t-1}\mathbf{S}_t' + \mathbf{D}_t^{-1}]^{-1}\mathbf{B}_t\mathbf{Q}_t^{-1}\mathbf{B}_t^{P'} \quad (3.21)$$

where $\mathbf{G}_t \equiv \mathbf{P}_{t|t-1}\mathbf{S}_t'(\mathbf{S}_t\mathbf{P}_{t|t-1}\mathbf{S}_t' + \mathbf{D}_t^{-1})^{-1}$ is the $r \times n_t$ Kalman gain matrix. $\mathbf{D}_t \equiv (\mathbf{B}_t\mathbf{Q}_t^{-1}\mathbf{B}_t' + \mathbf{V}_t)^{-1}$ is an n_t -by- n_t matrix. \mathbf{B}_t^P is the basis matrix in the GGM component, with (i, j) -th element being one if the i -th prediction location is the j -th BAU, and zero otherwise.

The smoothing algorithm is proceeded backwards in time for $t = T - 1, T - 2, \dots, 1$:

$$\boldsymbol{\eta}_{t|T} = \boldsymbol{\eta}_{t|t} + \mathbf{J}_t(\boldsymbol{\eta}_{t+1|T} - \boldsymbol{\eta}_{t+1|t}) \quad (3.22)$$

$$\mathbf{P}_{t|T} = \mathbf{P}_{t|t} + \mathbf{J}_t(\mathbf{P}_{t+1|T} - \mathbf{P}_{t+1|t})\mathbf{J}_t' \quad (3.23)$$

$$\boldsymbol{\delta}_{t|T}^P = \boldsymbol{\delta}_{t|t}^P + \mathbf{M}_t(\boldsymbol{\eta}_{t+1|T} - \boldsymbol{\eta}_{t+1|t}) \quad (3.24)$$

$$\mathbf{R}_{t|T}^P = \mathbf{R}_{t|t}^P + \mathbf{M}_t(\mathbf{P}_{t+1|T} - \mathbf{P}_{t+1|t})\mathbf{M}_t' \quad (3.25)$$

where

$$\mathbf{J}_t \equiv \mathbf{P}_{t|t}\mathbf{H}_{t+1}'\mathbf{P}_{t+1|t}^{-1}$$

$$\mathbf{M}_t \equiv -\mathbf{B}_t^P\mathbf{Q}_t^{-1}\mathbf{B}_t'\mathbf{G}_t'\mathbf{H}_{t+1}'\mathbf{P}_{t+1|t}^{-1}.$$

The smoothing distribution of the initial state $\boldsymbol{\eta}_0$ is

$$\boldsymbol{\eta}_{0|T} = \boldsymbol{\eta}_{0|0} + \mathbf{J}_0(\boldsymbol{\eta}_{1|T} - \boldsymbol{\eta}_{1|0})$$

$$\mathbf{P}_{0|T} = \mathbf{P}_{0|0} + \mathbf{J}_0(\mathbf{P}_{1|T} - \mathbf{P}_{1|0})\mathbf{J}_0'.$$

The lag-1 cross-covariance term $\mathbf{P}_{t,t-1|T} \equiv \text{cov}(\boldsymbol{\eta}_t, \boldsymbol{\eta}_{t-1} \mid \mathbf{Z}_{1:T})$ is given by

$$\mathbf{P}_{T,T-1|T} = (\mathbf{I}_r - \mathbf{G}_T\mathbf{S}_T')\mathbf{H}_T\mathbf{P}_{T-1|T-1} \quad (3.26)$$

$$\mathbf{P}_{t,t-1|T} = \mathbf{P}_{t|t}\mathbf{J}_{t-1}' + \mathbf{J}_t(\mathbf{P}_{t+1,t|T} - \mathbf{P}_{t|t})\mathbf{J}_{t-1}', \quad t = T - 1, T - 2, \dots, 1. \quad (3.27)$$

3.2 Filtering Distribution for Hidden Process $Y_t(\cdot)$

For $t = 1, \dots, T$, the optimal filter of \mathbf{Y}_t^P given the data $\mathbf{Z}_{1:t}$, denoted by $\mathbf{Y}_{t|t}^P$, is

$$\mathbf{Y}_{t|t}^P \equiv E(\mathbf{Y}_t^P \mid \mathbf{Z}_{1:t}) = \mathbf{X}_t^P \boldsymbol{\beta}_t + \mathbf{S}_t^P \boldsymbol{\eta}_{t|t} + \boldsymbol{\delta}_{t|t}^P, \quad (3.28)$$

where $\boldsymbol{\eta}_{t|t}$ is given in Eq. (3.18), and $\boldsymbol{\delta}_{t|t}^P$ is given in Eq. (3.20). We call (3.28) the *DFGPF (Dynamic Fused Gaussian Process Filter)*. Its associated mean-squared-prediction-error covariance matrix is

$$\begin{aligned} \sigma_{t|t}^2 &\equiv E\{[\mathbf{Y}^P - \mathbf{Y}_{t|t}^P][\mathbf{Y}^P - \mathbf{Y}_{t|t}^P]'\} \\ &= \mathbf{S}_t^P \mathbf{P}_{t|t} \mathbf{S}_t^{P'} + \mathbf{R}_{t|t}^P + \mathbf{S}_t^P \mathbf{C}_{t|t} + (\mathbf{S}_t^P \mathbf{C}_{t|t})', \end{aligned} \quad (3.29)$$

where $\mathbf{C}_{t|t} \equiv \text{cov}(\boldsymbol{\eta}_t, \boldsymbol{\delta}_t^P \mid \mathbf{Z}_{1:t}) = -\mathbf{G}_t \mathbf{B}_t \mathbf{Q}_t^{-1} \mathbf{B}_t^{P'}$. We call the square root of the diagonal elements in $\sigma_{t|t}^2$ the DFGPF standard errors.

3.3 Smoothing Distribution for Hidden Process $Y_t(\cdot)$

For $t = 1, \dots, T - 1$, the optimal smoother of \mathbf{Y}_t^P given the data $\mathbf{Z}_{1:T}$, denoted by $\mathbf{Y}_{t|T}^P$, is

$$\mathbf{Y}_{t|T}^P \equiv E(\mathbf{Y}_t^P \mid \mathbf{Z}_{1:T}) = \mathbf{X}_t^P \boldsymbol{\beta}_t + \mathbf{S}_t^P \boldsymbol{\eta}_{t|T} + \boldsymbol{\delta}_{t|T}^P, \quad (3.30)$$

where $\boldsymbol{\eta}_{t|T}$ is given in Eq. (3.22), and $\boldsymbol{\delta}_{t|T}^P$ is given in Eq. (3.24). We call (3.30) the *DFGPS (Dynamic Fused Gaussian Process Smoother)*. Its associated mean-squared-prediction-error covariance matrix is

$$\sigma_{t|T}^2 \equiv E\{[\mathbf{Y}^P - \mathbf{Y}_{t|T}^P][\mathbf{Y}^P - \mathbf{Y}_{t|T}^P]'\} \quad (3.31)$$

$$= \mathbf{S}_t^P \mathbf{P}_{t|T} \mathbf{S}_t^{P'} + \mathbf{R}_{t|T}^P + \mathbf{S}_t^P \mathbf{C}_{t|T} + (\mathbf{S}_t^P \mathbf{C}_{t|T})', \quad (3.32)$$

where $\mathbf{C}_{t|T} \equiv \text{cov}(\boldsymbol{\eta}_t, \boldsymbol{\delta}_t^P \mid \mathbf{Z}_{1:T}) = -\mathbf{G}_t \mathbf{B}_t \mathbf{Q}_t^{-1} \mathbf{B}_t^{P'} + \mathbf{J}_t (\mathbf{P}_{t+1|T} - \mathbf{P}_{t+1|t}) \mathbf{M}_t'$. We call the square root of the diagonal elements in $\sigma_{t|T}^2$ the DFGPS standard errors.

4 Maximum Likelihood Estimation via Stochastic EM Algorithm

In what follows, we will give a general derivation of the maximum likelihood estimation procedure for both filtering and smoothing methodology based on DFGP. Let u denote a generic time point. For the filtering-type estimator, the parameters will be estimated based on data $\mathbf{Z}_{1:u}$, where u takes values from 2 to T , since data are collected from time point 1 to time point T . For the smoothing-type estimator, the parameters will be estimated based on the data $\mathbf{Z}_{1:u}$, where u takes value T only, since all the data should be used in the smoothing-type methodology. To avoid identifiability issues, we assume that the propagation matrices $\{\mathbf{H}_t : t = 1, \dots, T\}$ and innovation matrices $\{\mathbf{U}_t : t = 1, \dots, T\}$ are time-invariant. Let $\boldsymbol{\theta} \equiv \{\boldsymbol{\beta}_1, \dots, \boldsymbol{\beta}_u, \mathbf{K}_0, \mathbf{H}, \mathbf{U}, \tau_1^2, \dots, \tau_u^2, \gamma_1, \dots, \gamma_u\} \cup \{\sigma_{\epsilon_t, (k)}^2 : t = 1, \dots, u; k = 1, \dots, k_0\}$ be a collection of model parameters up to time u . If the goal is to make filtering-type predictions, the letter u denotes the current time at which predictions will be made, and parameters are estimated based on data up to current time u . If the goal is to make smoothing-type predictions, the letter u denotes the time at which latest data are observed at time T . Smoothing-type predictions will be made at time $t = 1, \dots, T-1$. In what follows, we will give an efficient parameter estimation procedure to ensure the scalability of the DFGP methodology for massive datasets.

4.1 Likelihood Function

Let $\boldsymbol{\alpha}_t = \mathbf{Z}_t - \mathbf{X}_t \boldsymbol{\beta}_t - \mathbf{S}_t \boldsymbol{\eta}_{t|t-1}$ be innovations for $t = 1, \dots, u$. These innovations are independently and normally distributed with mean zero and covariance matrix $\boldsymbol{\Sigma}_{t|t-1} = \mathbf{S}_t \mathbf{P}_{t|t-1} \mathbf{S}_t' + \mathbf{D}_t^{-1}$. Then, up to a constant, the negative twice marginal log-likelihood function is

$$-2 \ln L(\boldsymbol{\theta}) = -2f(\boldsymbol{\alpha}_1, \dots, \boldsymbol{\alpha}_u | \boldsymbol{\theta}) = \sum_{t=1}^u \ln |\boldsymbol{\Sigma}_{t|t-1}| + \sum_{t=1}^u \boldsymbol{\alpha}_t(\boldsymbol{\theta})' \boldsymbol{\Sigma}_{t|t-1}(\boldsymbol{\theta})^{-1} \boldsymbol{\alpha}_t(\boldsymbol{\theta}), \quad (4.1)$$

where $\boldsymbol{\theta}$ denotes model parameters. The inverse and log-determinant of $\boldsymbol{\Sigma}_{t|t-1}$ can be calculated as follows:

$$\boldsymbol{\Sigma}_{t|t-1}^{-1} = \mathbf{D}_t - \mathbf{D}_t \mathbf{S}_t (\mathbf{P}_{t|t-1}^{-1} + \mathbf{S}_t' \mathbf{D}_t \mathbf{S}_t)^{-1} \mathbf{S}_t' \mathbf{D}_t \quad (4.2)$$

$$\ln |\boldsymbol{\Sigma}_{t|t-1}| = \ln |\mathbf{P}_{t|t-1}^{-1} + \mathbf{S}_t' \mathbf{D}_t \mathbf{S}_t| + \ln |\mathbf{P}_{t|t-1}| + \ln |\mathbf{D}_t^{-1}|, \quad (4.3)$$

where $\mathbf{D}_t = \mathbf{V}_t^{-1} - \mathbf{V}_t^{-1}\mathbf{B}_t(\mathbf{Q}_t + \mathbf{B}_t'\mathbf{V}_t^{-1}\mathbf{B}_t)^{-1}\mathbf{B}_t'\mathbf{V}_t^{-1}$ and $\ln |\mathbf{D}_t^{-1}| = \ln |\mathbf{Q}_t + \mathbf{B}_t'\mathbf{V}_t^{-1}\mathbf{B}_t| - \ln |\mathbf{Q}_t^{-1}| + \ln |\mathbf{V}_t|$. To evaluate the negative twice marginal log-likelihood function in Eq. (4.1), solving linear systems involving $\Sigma_{t|t-1}$ are required. To solve $\Sigma_{t|t-1}^{-1}\mathbf{T}$ for a n_t -dimensional vector or a n_t -by- r matrix \mathbf{T} , ones has to solve linear systems involving r -by- r matrices and N -by- N sparse matrix $\mathbf{Q}_t + \mathbf{B}_t'\mathbf{V}_t^{-1}\mathbf{B}_t$. The former requires $O(r^3)$ computational cost. If the sparse matrix $\mathbf{Q}_t + \mathbf{B}_t'\mathbf{V}_t^{-1}\mathbf{B}_t$ has bandwidth p_0 after appropriate reordering, the computational cost of the Cholesky decomposition for $\mathbf{Q}_t + \mathbf{B}_t'\mathbf{V}_t^{-1}\mathbf{B}_t$ is $O(N(p_0^2 + 3p_0))$. Linear systems involving $\mathbf{Q}_t + \mathbf{B}_t'\mathbf{V}_t^{-1}\mathbf{B}_t$ can be solved efficiently. The Cholesky decomposition of \mathbf{Q} can be solved very efficiently with $O(N^{1.5})$ computational cost (e.g., Ma and Kang, 2018).

4.2 Stochastic EM Algorithm

The expectation-maximization (EM) algorithm introduced by Dempster et al. (1977) is a powerful method to solve maximum likelihood estimation problems iteratively, where the E-step is calculated exactly, and then followed by an M-step in each iteration. Instead of computing the conditional expectation exactly in E-step, one can employ the Monte Carlo algorithm to generate samples from the conditional distribution, and then replace the conditional expectation with an average of corresponding quantities evaluated at these samples. This estimation method is called the Monte Carlo EM algorithm (Wei and Tanner, 1990). The success of the Monte Carlo EM algorithm relies on sufficiently large samples to approximate the E-step conditional expectations. A closely related modification of the EM algorithm described in Celeux and Diebolt (1985) is known as the stochastic EM (SEM) algorithm, which substitutes the E-step with a single corresponding quantity evaluated with one random sample from the conditional distribution. The SEM algorithm is generally less computationally expensive than the Monte Carlo EM algorithm, and is asymptotically equivalent to the EM algorithm under certain conditions (see Nielsen, 2000; Marschner, 2001, for details). In what follows, we give the SEM procedure to estimate parameters in DFGP.

Up to a constant, the negative twice complete log-likelihood is

$$\begin{aligned}
-2 \ln L_c(\boldsymbol{\theta}) &= -2 \ln f(\mathbf{Z}_{1:u}, \boldsymbol{\eta}_{0:u}, \boldsymbol{\xi}_{1:u} | \boldsymbol{\theta}) \\
&= \sum_{t=1}^u \{ (\mathbf{Z}_t - \mathbf{X}_t \boldsymbol{\beta}_t - \mathbf{S}_t \boldsymbol{\eta}_t - \mathbf{B}_t \boldsymbol{\xi}_t)' \mathbf{V}_t^{-1} (\mathbf{Z}_t - \mathbf{X}_t \boldsymbol{\beta}_t - \mathbf{S}_t \boldsymbol{\eta}_t - \mathbf{B}_t \boldsymbol{\xi}_t) \} \\
&+ \sum_{t=1}^u \{ (\boldsymbol{\eta}_t - \mathbf{H}_t \boldsymbol{\eta}_{t-1})' \mathbf{U}_t^{-1} (\boldsymbol{\eta}_t - \mathbf{H}_t \boldsymbol{\eta}_{t-1}) + \ln |\mathbf{U}_t| \} \\
&+ \ln |\mathbf{K}_0| + \boldsymbol{\eta}_0' \mathbf{K}_0^{-1} \boldsymbol{\eta}_0 + \sum_{t=1}^u \{ \boldsymbol{\xi}_t' \mathbf{Q}_t \boldsymbol{\xi}_t - \ln |\mathbf{Q}_t| + \ln |\mathbf{V}_t| \}.
\end{aligned} \tag{4.4}$$

Given the negative twice complete log-likelihood function in Eq. (4.4), we now derive the Q -function in the EM algorithm first, and then present the derivation for the SEM algorithm. Consider the $(\ell + 1)$ th iteration in the EM algorithm. The expectation step is to find conditional expectation of the complete log-likelihood for $\boldsymbol{\theta} = \boldsymbol{\theta}^{[\ell]}$ with respect to missing data, i.e., $Q(\boldsymbol{\theta}; \boldsymbol{\theta}^\ell) := E_{\boldsymbol{\theta}^{[\ell]}}[-2 \ln L_c(\boldsymbol{\theta}) | \mathbf{Z}_{1:u}]$. In what follows, the following notations are used: $\boldsymbol{\eta}_{t|u}^{[\ell]} = E_{\boldsymbol{\theta}^{[\ell]}}(\boldsymbol{\eta}_t | \mathbf{Z}_{1:u})$, $\boldsymbol{\delta}_{t|u}^{[\ell]} = E_{\boldsymbol{\theta}^{[\ell]}}(\boldsymbol{\delta}_t | \mathbf{Z}_{1:u})$, $\mathbf{P}_{t|u}^{[\ell]} = \text{var}(\boldsymbol{\eta}_t | \mathbf{Z}_{1:u}, \boldsymbol{\theta}^{[\ell]})$, $\mathbf{R}_{t|u}^{[\ell]} = \text{var}(\boldsymbol{\delta}_t | \mathbf{Z}_{1:u}, \boldsymbol{\theta}^{[\ell]})$, $\mathbf{P}_{t,t-1|u}^{[\ell]} = \text{cov}(\boldsymbol{\eta}_t, \boldsymbol{\eta}_{t-1} | \mathbf{Z}_{1:u}, \boldsymbol{\theta}^{[\ell]})$ for all t . In EM algorithm, the actual prediction location \mathcal{D}^P is the same as observed locations, \mathcal{D}^O , for $t = 1, \dots, u$. We also define the quantities $\mathbf{K}_t^{[\ell+1]} \equiv \mathbf{P}_{t|u}^{[\ell]} + \boldsymbol{\eta}_{t|u}^{[\ell]} \boldsymbol{\eta}_{t|u}^{[\ell]}'$ and $\mathbf{L}_t^{[\ell+1]} \equiv \mathbf{P}_{t,t-1|u}^{[\ell]} + \boldsymbol{\eta}_{t|u}^{[\ell]} \boldsymbol{\eta}_{t-1|u}^{[\ell]}'$.

In the EM algorithm, these conditional expectations are computed exactly; while in the SEM algorithm, they are replaced by the complete log-likelihood function evaluated with a single sample from the posterior distribution $[\boldsymbol{\eta}_t, \boldsymbol{\xi}_t | \mathbf{Z}_{1:u}]$. To ensure the positive definiteness of matrices $\mathbf{K}_0^{[\ell]}$ and $\mathbf{U}_0^{[\ell]}$, we compute the conditional expectations involving them exactly. We only use samples from $[\boldsymbol{\eta}_t, \boldsymbol{\xi}_t | \mathbf{Z}_{1:u}, \boldsymbol{\theta}^{[\ell]}]$ to approximate the conditional expectations involving in $\boldsymbol{\xi}_t$ by their samples. That is, we compute conditional expectations involving $\boldsymbol{\eta}_t$ explicitly, and we define $\boldsymbol{\eta}_{t|u}^{[\ell]} = E_{\boldsymbol{\theta}^{[\ell]}}(\boldsymbol{\eta}_t | \mathbf{Z}_{1:u})$. For expectations involving $\boldsymbol{\xi}_t$, we generate a sample from $[\boldsymbol{\eta}_t, \boldsymbol{\xi}_t | \mathbf{Z}_{1:u}, \boldsymbol{\theta}^{[\ell]}]$, and use $\boldsymbol{\xi}_{t|u}^{[\ell]}$ to denote a sample for $\boldsymbol{\xi}_t$ from the distribution $[\boldsymbol{\eta}_t, \boldsymbol{\xi}_t | \mathbf{Z}_{1:u}, \boldsymbol{\theta}^{[\ell]}]$. To generate a sample from the distribution $[\boldsymbol{\eta}_t, \boldsymbol{\xi}_t | \mathbf{Z}_{1:u}, \boldsymbol{\theta}^{[\ell]}]$, we use the conditional simulation strategy in geostatistics to allow fast sampling procedure (for details, see Cressie, 1993, Sec. 3.6.2).

The negative twice $Q_{SEM}(\cdot; \cdot)$ function in SEM algorithm is

$$\begin{aligned}
-2Q_{SEM}(\boldsymbol{\theta}; \boldsymbol{\theta}^\ell) &\equiv \sum_{t=1}^u \left\{ (\mathbf{Z}_t - \mathbf{X}_t \boldsymbol{\beta}_t - \mathbf{S}_t \boldsymbol{\eta}_{t|u}^{[\ell]} - \mathbf{B}_t \boldsymbol{\xi}_{t|u}^{[\ell]})' \mathbf{V}_t^{-1} (\mathbf{Z}_t - \mathbf{X}_t \boldsymbol{\beta}_t - \mathbf{S}_t \boldsymbol{\eta}_{t|u}^{[\ell]} - \mathbf{B}_t \boldsymbol{\xi}_{t|u}^{[\ell]}) \right\} \\
&+ u \ln |\mathbf{U}| + \sum_{t=1}^u \text{tr} \left\{ \mathbf{U}_t^{-1} (\mathbf{K}_t^{[\ell+1]} - \mathbf{H} \mathbf{L}_t^{[\ell+1]'} - \mathbf{L}_t^{[\ell+1]} \mathbf{H}' + \mathbf{H} \mathbf{K}_{t-1}^{[\ell+1]} \mathbf{H}') \right\} \\
&+ \ln |\mathbf{K}_0| + \text{tr}(\mathbf{K}_0 \mathbf{K}_0^{[\ell+1]}) + \sum_{t=1}^u \left\{ \boldsymbol{\xi}_{t|u}^{[\ell]'} \mathbf{Q}_t \boldsymbol{\xi}_{t|u}^{[\ell]} - \ln |\mathbf{Q}_t| + \ln |\mathbf{V}_t| \right\},
\end{aligned}$$

where $\boldsymbol{\xi}_{t|u}^{[\ell]}$ is the sub-vector of a random sample from $[\boldsymbol{\eta}_t, \boldsymbol{\xi}_t \mid \mathbf{Z}_{1:u}, \boldsymbol{\theta}^{[\ell]}]$ corresponding to $\boldsymbol{\xi}_t$. We compute the expectations involving \mathbf{U}_t and \mathbf{K}_0 exactly, since this will give a desirable property in their updating formulas that both of them are guaranteed to be positive definite in each iteration of the SEM algorithm.

In the M-step, this Q_{SEM} function is maximized with respect to parameters $\boldsymbol{\theta}$, yielding the following formulas to update parameters for $t = 1, \dots, u$:

$$\begin{aligned}
\boldsymbol{\beta}_t^{[\ell+1]} &= (\mathbf{X}_t' \mathbf{V}_t \mathbf{X}_t)^{-1} \mathbf{X}_t' \mathbf{V}_t^{-1} (\mathbf{Z}_t - \mathbf{S}_t \boldsymbol{\eta}_{t|u}^{[\ell]} - \mathbf{B}_t \boldsymbol{\xi}_{t|u}^{[\ell]}) \\
\sigma_{\epsilon_t, (k)}^{2[\ell+1]} &= \left\{ (\mathbf{Z}_t^{(k)} - \mathbf{X}_t^{(k)} \boldsymbol{\beta}_t^{[\ell+1]} - \mathbf{S}_t^{(k)} \boldsymbol{\eta}_{t|u}^{[\ell]} - \mathbf{B}_t^{(k)} \boldsymbol{\xi}_{t|u}^{[\ell]})' \mathbf{V}_{\epsilon_t, (k)}^{-1} \right. \\
&\quad \cdot \left. (\mathbf{Z}_t^{(k)} - \mathbf{X}_t^{(k)} \boldsymbol{\beta}_t^{[\ell+1]} - \mathbf{S}_t^{(k)} \boldsymbol{\eta}_{t|u}^{[\ell]} - \mathbf{B}_t^{(k)} \boldsymbol{\xi}_{t|u}^{[\ell]}) \right\} / n_t^{(k)} \\
\mathbf{K}_0^{[\ell+1]} &= \mathbf{P}_{0|u}^{[\ell]} + \boldsymbol{\eta}_{0|u}^{[\ell]} \boldsymbol{\eta}_{0|u}^{[\ell]'} \\
\mathbf{H}^{[\ell+1]} &= \left(\sum_{t=1}^u \mathbf{L}_t^{[\ell+1]} \right) \left(\sum_{t=0}^{u-1} \mathbf{K}_t^{[\ell+1]} \right)^{-1} \\
\mathbf{U}^{[\ell+1]} &= \left(\sum_{t=1}^u \mathbf{K}_t^{[\ell+1]} - \mathbf{H}^{[\ell+1]} \sum_{t=1}^u \mathbf{L}_t^{[\ell+1]'} \right) / u \\
\tau_t^{2[\ell+1]} &= \boldsymbol{\xi}_{t|u}^{[\ell]'} (\mathbf{I} - \gamma_t^{[\ell]} \mathbf{W}) \boldsymbol{\xi}_{t|u}^{[\ell]} / N,
\end{aligned}$$

where the parameters $\boldsymbol{\beta}_t$, $\sigma_{\epsilon_t, (k)}^2$, \mathbf{K}_0 , \mathbf{H} , \mathbf{U} , and τ_t^2 have closed-form updates. When the M-step is carried out w.r.t. $\{\gamma_t : t = 1, \dots, u\}$, there is no explicit formula to update $\{\gamma_t : t = 1, \dots, u\}$. It is straightforward to show that we can minimize the following function w.r.t. these parameters:

$$g(\gamma_1, \dots, \gamma_u) = \sum_{t=1}^u \left(-\gamma_t \boldsymbol{\xi}_{t|u}^{[\ell]'} \mathbf{W} \boldsymbol{\xi}_{t|u}^{[\ell]} / \tau_t^{2[\ell]} - \ln |\mathbf{I} - \gamma_t \mathbf{W}| \right).$$

To solve this nonlinear optimization problem, we use the interior-point method; see Byrd et al. (1999) for details. Notice that we can estimate all the parameters including the nugget variance

parameters $\{\sigma_{\epsilon_t, (k)}^2 : t = 1, \dots, u; k = 1, \dots, k_0.\}$ in the SEM algorithm.

The SEM algorithm starts with certain initial values for the parameters θ , and then these parameters are updated iteratively at each iteration. The initial values should be tuned to achieve better convergence results. Here, we give some practical suggestions. The initial values of regression coefficients can be set as the ordinary least square estimates. The initial values for $\{\sigma_{\epsilon_t, (k)}^2 : t = 1, \dots, u; k = 1, \dots, k_0.\}$ can be set as the parameter estimates by fitting empirical semivariograms near origin (e.g., Kang et al., 2010). The initial values for \mathbf{K}_0 and \mathbf{U} can be set to the r -by- r positive definite matrices with diagonal entries adjusted by the empirical variance of the data values $\{\mathbf{Z}_t : t = 1, \dots, u\}$. The initial values for τ_t^2 can be set as a small portion (say 0.01) of the empirical variance of the data values $\{\mathbf{Z}_t : t = 1, \dots, u\}$. The initial values for \mathbf{H} can be set as an identity matrix. After the initial values are specified, the SEM algorithm will update them in each iteration. The formulas to update all these parameters reveal that the positive definiteness of matrix \mathbf{K} and \mathbf{U} is guaranteed. To check the convergence of the SEM algorithm, we can monitor the change or relative change of log-likelihood function (4.1) in two consecutive iterations.

Although the procedure to obtain standard errors for the parameter estimates is not discussed here, these standard errors can be obtained in a certain way. For instance, one might use the bootstrap-sampling technique described in Stoffer and Wall (1991) to compute the standard errors for these parameters estimates. Its detailed discussion is beyond the scope of this work. As in each iteration of the SEM algorithm, solving linear systems involving r -by- r matrices and N -by- N sparse matrices is required. We also need to carry out numerical optimization to update $\{\gamma_t : t = 1, \dots, u\}$, which requires the Cholesky decomposition for sparse matrices $\{\mathbf{Q}_t : t = 1, \dots, u\}$. These computations can be done efficiently but still require considerable amount of computational time.

When data are sparse, we can impose the time-invariant assumption for the nugget variance parameters $\{\sigma_{\epsilon_t, (k)}^2 : t = 1, \dots, u; k = 1, \dots, k_0.\}$ so that stable estimates for these parameters can be obtained. Suppose that $\sigma_{\epsilon, (k)}^2 \equiv \sigma_{\epsilon_1, (k)}^2 = \dots = \sigma_{\epsilon_u, (k)}^2$. The formulas to update these nugget variance parameters are:

$$\begin{aligned} \sigma_{\epsilon, (k)}^{2[\ell+1]} &= \sum_{t=1}^u \left\{ (\mathbf{Z}_t^{(k)} - \mathbf{X}_t^{(k)} \boldsymbol{\beta}_t^{[\ell+1]} - \mathbf{S}_t^{(k)} \boldsymbol{\eta}_{t|u}^{[\ell]} - \mathbf{B}_t^{(k)} \boldsymbol{\xi}_{t|u}^{[\ell]})' \mathbf{V}_{\epsilon_t, (k)}^{-1} \right. \\ &\quad \left. \cdot (\mathbf{Z}_t^{(k)} - \mathbf{X}_t^{(k)} \boldsymbol{\beta}_t^{[\ell+1]} - \mathbf{S}_t^{(k)} \boldsymbol{\eta}_{t|u}^{[\ell]} - \mathbf{B}_t^{(k)} \boldsymbol{\xi}_{t|u}^{[\ell]}) \right\} / \left(\sum_{t=1}^u n_t^{(k)} \right). \end{aligned}$$

When data are available over a large number of time steps, i.e., u is large, we can relax the time-invariant assumption for propagation matrices $\{\mathbf{H}_t : t = 1, \dots, u\}$, and innovation matrices $\{\mathbf{U}_t : t = 1, \dots, u\}$. Suppose that the propagation matrix and innovation matrix are constant over b_0 block time periods. Let $T_0 \equiv 0$ and $T_{b_0} \equiv u$. We further assume that $\mathbf{H}_1 = \dots = \mathbf{H}_{T_1} \neq \mathbf{H}_{T_1+1} = \dots = \mathbf{H}_{T_2} \neq \dots = \mathbf{H}_{T_{b_0}}$ and $\mathbf{U}_1 = \dots = \mathbf{U}_{T_1} \neq \mathbf{U}_{T_1+1} = \dots = \mathbf{U}_{T_2} \neq \dots = \mathbf{U}_{T_{b_0}}$. For $b = 1, \dots, b_0$, the formulas to update \mathbf{H}_{T_b} and \mathbf{U}_{T_b} are

$$\begin{aligned}\mathbf{H}_{T_b}^{[\ell+1]} &= \left(\sum_{t=T_{b-1}+1}^{T_b} \mathbf{L}_t^{[\ell+1]} \right) \left(\sum_{t=T_{b-1}+1}^{T_{b-1}} \mathbf{K}_t^{[\ell+1]} \right)^{-1}, \\ \mathbf{U}_{T_b}^{[\ell+1]} &= \left(\sum_{t=T_{b-1}+1}^{T_b} \mathbf{K}_t^{[\ell+1]} - \mathbf{H}^{[\ell+1]} \sum_{t=T_{b-1}+1}^{T_b} \mathbf{L}_t^{[\ell+1]'} \right) / (T_b - T_{b-1}).\end{aligned}$$

5 Results

What follows is to demonstrate our proposed DFGP methodology based on two SST datasets from MODIS and AMSR-E instruments. The tropical Pacific region is covered by $N = 1,260,864$ grid cells at 9km resolution, which are used to define BAUs in this study. These two SST datasets have been biased-corrected to ensure that the mean zero assumption in the measurement-error process is valid in the DFGP methodology. Exploratory analysis suggests that the covariates $\mathbf{X}_t(\cdot) = [1, \text{latitude}(\cdot), \text{latitude}(\cdot)^2]$ be included in the trend component for all time points. What follows is to demonstrate the filtering procedure of the DFGP methodology based upon massive amount of two SST datasets, and to make comparisons with other existing methods. In the following numerical illustrations, to assess the predictive performance for each method, we use the root-mean-squared-prediction error (RMSPE) to evaluate the accuracy of the predictions at held-out locations. We also use the continuous-rank-probability score (CRPS; Gneiting and Raftery, 2007) to quantify the uncertainties in the predictive distribution for held-out locations, where small value of the CRPS indicates less uncertainty in the predictive distribution.

5.1 Cross-Validation

We first carry out cross-validation to evaluate the filtering-type DFGP methodology and compare it with the spatio-temporal data fusion model in Nguyen et al. (2014). In what follows, we refer

to the spatio-temporal data fusion model in Nguyen et al. (2014) as *FRF*, and we refer to our filtering procedure of the DFGP methodology as *DFGPF*. In *FRF*, we consider 99 equally-spaced basis functions at three different resolutions and 181 equally-space basis functions at four different resolutions with previous 99 basis functions included. As an additional comparison, we also implement a local kriging approach (e.g., Haas, 1990; Vecchia, 1988), which makes predictions based on observations in a moving window. This approach has been widely used in practice to make spatial/spatio-temporal predictions due to its computational efficiency and the usage of spatial/spatio-temporal varying covariance functions in a local moving window. In our implementation of the local kriging approach, we fit an exponential covariance function model with its parameters estimated by the maximum likelihood method in a moving window such that it contains 30 nearest observations. This approach will be referred to as Local Kriging hereafter. Notice that when implementing the local kriging approach, we assume that each observation is associated with the centroid of the grid cell, and we ignore the resolution differences among each dataset.

To set up the cross-validation exercise, we hold out MODIS SST in the block region between longitude 180° and 190° and between latitude -20° and 0° for time point $t = 2, \dots, 8$; see Figure 2 for an example of the held-out region on Jan 8, 2018. This large contiguous region is used to test long-range prediction skills that are often required to make predictions for remote sensing data, because remote-sensing data often have missing latitude bands when polar-orbiting satellite instruments collect the data around the Earth. In addition, we also hold out randomly sampled 10% of remaining MODIS SST observations for time point $t = 2, \dots, 8$. This randomly held-out prediction locations will be used to test the short-range prediction skills. As our focus is to compare filtering-type predictions among Local Kriging, *FRF* and *DFGPF*, we only use the data up to time t to estimate parameters and to make filtering predictions at held-out locations at time t , where $t = 2, \dots, 8$. Notice that we do not hold out observations at time $t = 1$, since the filtering-type DFGP methodology reduces to the spatial-only FGP methodology, which has been studied in Ma and Kang (2018) under various numerical examples.

Figure 3 shows the RMSPE and CRPS for *FRF* and *DFGPF* at time point $t = 2, \dots, 8$. As we can see, *DFGPF* performs the best among all the three methods in terms of RMSPE and CRPS at all time points. Even though the number of basis functions in the low-rank component of *FRF* is almost twice as that in *DFGPF*, *DFGPF* still outperforms *FRF* in terms of RMSPE and CRPS at all

time points, since the DFGPF model incorporates a more flexible covariance function than that in the FRF model.

The Local Kriging approach gives better predictions than FRF with only 99 basis functions, but FRF with more basis functions (e.g., $r = 181$) will outperform Local Kriging. For instance, at time point $t = 7$, FRF with 181 basis functions gives better RMSPE and CRPS than Local Kriging. We did not discuss how FRF would perform better than Local Kriging by adding more basis functions or using adaptive basis functions; readers are referred to Ma et al. (2018) for details. DFGP outperforms Local Kriging at all tested time points in terms of RMSPE and CRPS. The reasons are as follows. First, Local Kriging fails to provide good predictions especially in large contiguous missing region, since it only uses local information without borrowing strength from distant observations. Second, Local Kriging uses a stationary exponential covariance function, which may not be flexible enough to capture nonstationary behavior of the underlying geophysical process. Third, Local Kriging does not address the change-of-support problem. It is shown in Ma et al. (2018) that ignoring the change-of-support problem may result in unfavorable statistical inferential results.

Table 1 shows the average of numerical measure such as RMSPE and CRPS across all the seven tested time points as well as the total computing time (in hours) for parameter estimation and prediction on a 10-core machine with 20GB memory and Intel Xeon E5-2680 central processing unit. We see that DFGP outperforms Local Kriging and FRF in terms of RMSPE and CRPS. FRF with 181 basis functions outperforms Local Kriging in terms of RMSPE and CRPS on average. For the computational time, FRF with $r = 99$ is fastest, since FRF only needs to invert r -by- r matrix and diagonal matrix. When r is very small (e.g., $r = 99$), its computation can be very fast. Local Kriging is second fastest, since it only needs to solve very small (e.g., 30-by-30) linear systems for every prediction location, and the parallel computing environment can be employed to facilitate computations. DFGPF requires about 6 times more computational time than FRF, since DFGPF not only inverts r -by- r matrix but also needs to solve sparse linear systems for N -by- N sparse matrices. Even though DFGPF requires more computational time, it can give very good predictive performance in a reasonable amount of time, since DFGPF is able to process a 8-day dataset with about 3.7 million observations in a time much less than one week.

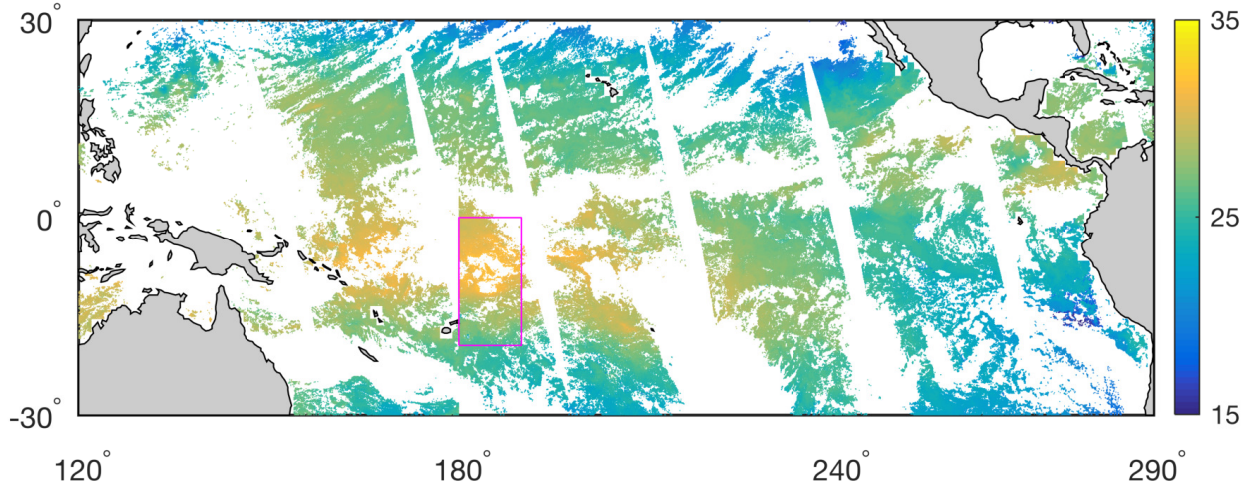


Figure 2. MODIS SST data are held out in the rectangular region on Jan 8, 2010. The delineated rectangular region is the held-out contiguous region to test long-range prediction skills.

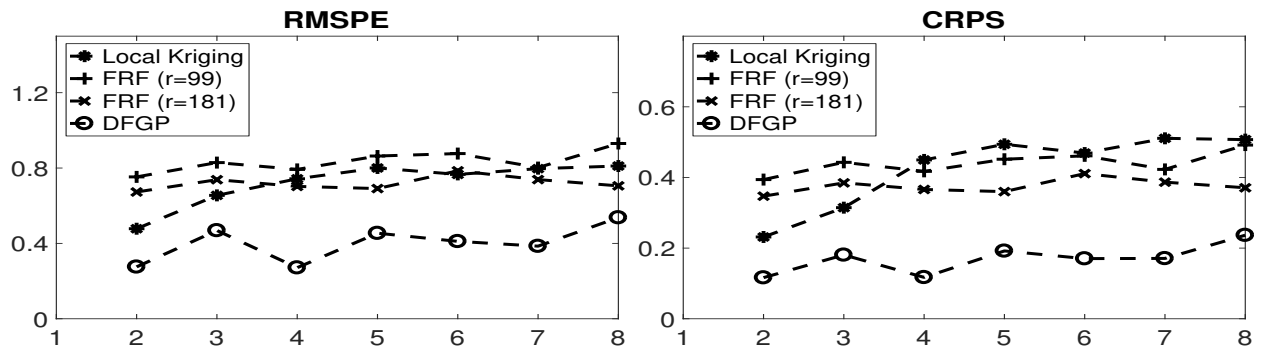


Figure 3. Numerical measures for predictions over all held-out locations based on Local Kriging, FRF, and DFGPF at $t = 2, \dots, 8$. The figure shows the RMSPEs at the left panel and CRPSs at the right panel for these methods, respectively. The asterisk represents the numerical measures based on Local Kriging; the plus sign represents the numerical measures based on FRF with $r = 99$ basis functions; the cross sign represents the numerical measures based on FRF with $r = 181$ basis functions; the circle sign represents the numerical measures based on DFGPF.

Table 1. Results in the cross-validation study. The RMSPE and CRPS are averaged over all held-out locations and all time points.

	Local Kriging	FRF $r = 99$	FRF $r = 181$	DFGPF $r = 99$
RMSPE	0.7214	0.8354	0.7191	0.4004
CRPS	0.4252	0.4402	0.3751	0.1692
Time (h)	4.5	2.4	6.5	22

5.2 Filtering Predictions for MODIS SST and AMSR-E SST

After carrying out cross-validation, we apply our DFGPF methodology to make filtering-type predictions for $t = 2, \dots, 8$. Based on estimated parameters, Figure 4 shows the filtered predictions for $t = 4, 6, 8$ and associated standard errors. As we can see, the resulting predictions are able to fill in the gaps by combining two sources of datasets. The associated prediction standard errors are also reasonable. We see that the predictions show larger uncertainties at locations where there are no SST data than those at locations where there are SST data. In the Supplementary Materials, we also included a movie to show the filtering type predictions for $t = 2, 3, \dots, 8$.

6 Conclusions and Discussion

In this article, we propose a dynamic fused Gaussian process model to allow both filtering and smoothing type predictions. The parameters in DFGP are estimated via an efficient stochastic expectation-maximization algorithm. Based on the DFGP methodology, we demonstrate the spatio-temporal data fusion model DFGPF with multiple data sources at different spatial resolutions. We have applied our DFGPF model to analyze massive amount of sea surface temperature data from MODIS and AMSR-E satellite instruments. We found that DFGPF gives better prediction results than the local kriging approach and the spatio-temporal data fusion model FRF. Although DFGPF requires more computational cost than Local Kriging and FRF, the computations in DFGPF can be done efficiently with affordable computing resources, since a one-week dataset can be processed in much less than one week for our massive amount of sea surface temperature data. By borrowing strength across different time and instruments, DFGPF is able to give good prediction results to fill in the gaps for massive amount of sea surface temperature data. Throughout the numerical illustrations, we focus on the filtering type of the DFGP methodology, i.e., DFGPF, and do not compare the smoothing type of the DFGP methodology, i.e., DFGPS, with other exiting work such as Fixed Rank Smoothing (Katzfuss and Cressie, 2011). A complete and thorough demonstration of DFGPS is left for future work.

The DFGP methodology assumes a single underlying true process, with the data process linked to this true process through different measurement-error processes. The resolution difference among each data process has been explicitly accounted for through the change-of-support prop-

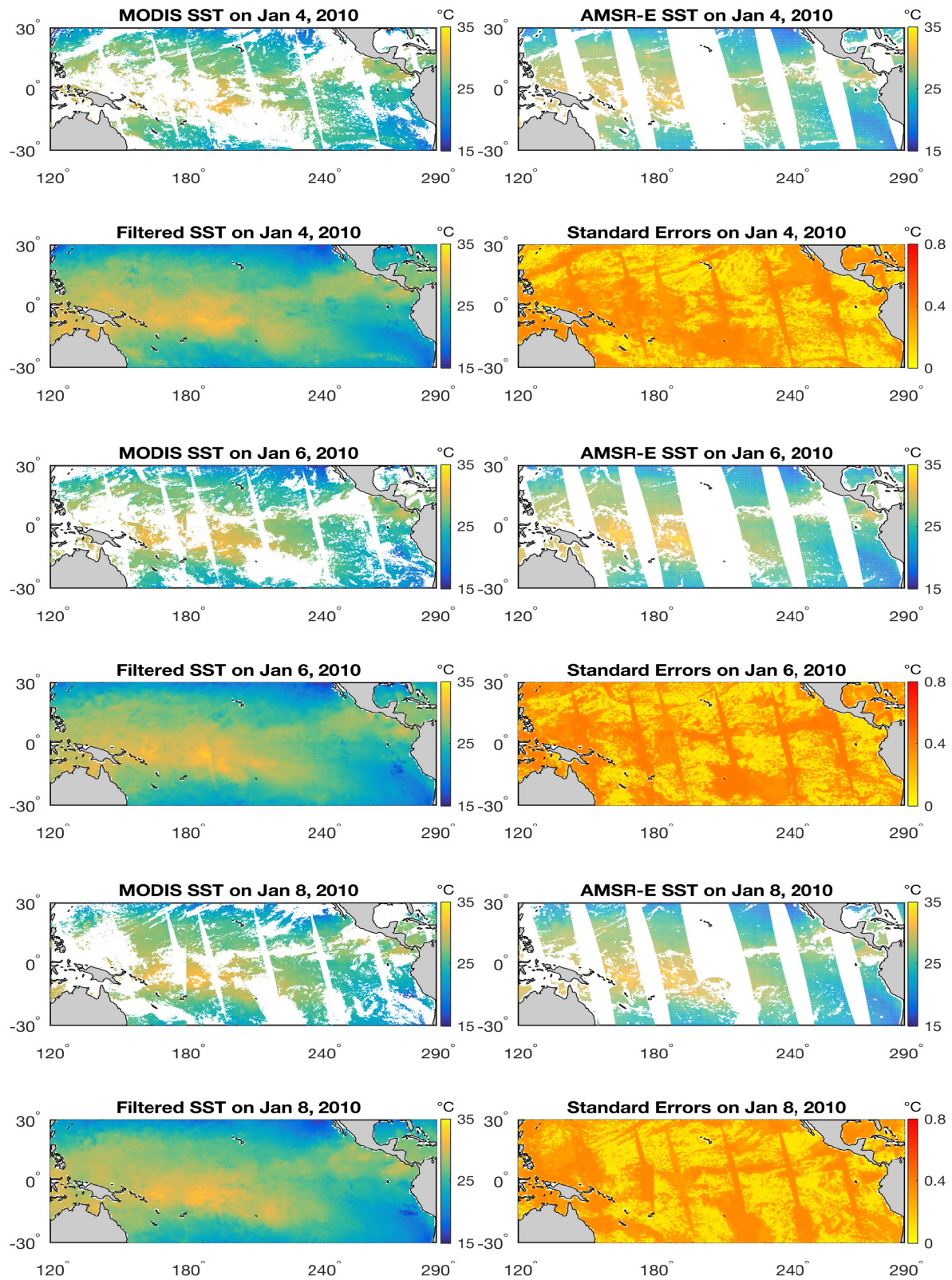


Figure 4. DFGP filtering predictions on Jan 4, 6, 8 in the year 2010 over the tropical Pacific ocean.

erty. When two different true processes are desired, one can extend the idea in Nguyen et al. (2014) to allow cross dependences among each underlying true process. In the DFGP methodology, the temporal dependence is only exhibited in the low-rank component, which captures large-scale spatio-temporal variations. Future work might be introducing temporal dependence structure in the graphical model component. These topics will be investigated in future research.

Acknowledgments

This material was based upon work partially supported by the National Science Foundation under Grant DMS-1638521 to the Statistical and Applied Mathematical Sciences Institute. Any opinions, findings, and conclusions or recommendations expressed in this material do not necessarily reflect the views of the National Science Foundation.

References

- Arai, K. (2013). Data fusion between microwave and thermal infrared radiometer data and its application to skin sea surface temperature, wind speed and salinity retrievals. *International Journal of Advanced Computer Science and Applications (IJACSA)*, 4(2).
- Berliner, L. M., Wikle, C. K., and Cressie, N. (2000). Long-lead prediction of Pacific SSTs via Bayesian dynamic modeling. *Journal of Climate*, 13(2):3953–3968.
- Berrocal, V. J., Gelfand, A. E., and Holland, D. M. (2010). A bivariate space-time downscaler under space and time misalignment. *The Annals of Applied Statistics*, 4(4):1942–1975.
- Berrocal, V. J., Gelfand, A. E., and Holland, D. M. (2012). Space-time data fusion under error in computer model output: An application to modeling air quality. *Biometrics*, 68(3):837–848.
- Byrd, R. H., Hribar, M. E., and Nocedal, J. (1999). An interior point algorithm for large-scale nonlinear programming. *SIAM Journal on Optimization*, 9(4):877–900.
- Celex, G. and Diebolt, J. (1985). The SEM algorithm: A probabilistic teacher algorithm derived from the EM algorithm for the mixture problem. *Computational Statistics Quarterly*, 2:73–82.
- Choi, J., Fuentes, M., and Reich, B. J. (2009). Spatial-temporal association between fine particulate matter and daily mortality. *Computational Statistics and Data Analysis*, 53(8):2989–3000.
- Cressie, N. (1993). *Statistics for Spatial Data*. John Wiley & Sons, New York, revised edition.
- Cressie, N. (1996). “Change of support and the modifiable areal unit problem”. *Geographical Systems*, 3(2-3):159–180.
- Cressie, N. and Johannesson, G. (2006). Spatial prediction for massive datasets, in mastering the data explosion in the earth and environmental sciences. In *Proceedings of the Australian*

- Academy of Science Elizabeth and Frederick White Conference*, page 11, Canberra, Australia. Australian Academy of Science.
- Cressie, N. and Johannesson, G. (2008). “Fixed rank kriging for very large spatial data sets”. *Journal of the Royal Statistical Society: Series B (Statistical Methodology)*, 70(1):209–226.
- Cressie, N., Shi, T., and Kang, E. L. (2010). Fixed rank filtering for spatio-temporal data. *Journal of Computational and Graphical Statistics*, 19(3):724–745.
- Cressie, N. and Wikle, C. K. (2002). Space-time Kalman filter. *Encyclopedia of environmetrics*.
- Cressie, N. and Wikle, C. K. (2011). *Statistics for Spatio-Temporal Data*. John Wiley & Sons, New York.
- Dempster, A. P., Laird, N. M., and Rubin, D. B. (1977). “Maximum likelihood from incomplete data via the EM algorithm”. *Journal of the Royal Statistical Society: Series B (Statistical Methodology)*, 39(1):1–38.
- Donlon, C. J., Minnett, P. J., Gentemann, C., Nightingale, T. J., Barton, I. J., Ward, B., and Murray, M. J. (2002). “Toward improved validation of satellite sea surface skin temperature measurements for climate research”. *Journal of Climate*, 15(4):353–369.
- Fuentes, M. and Raftery, A. E. (2005). Model evaluation and spatial interpolation by Bayesian combination of observations with outputs from numerical models. *Biometrics*, 61(1):36–45.
- Gelfand, A. E., Zhu, L., and Carlin, B. P. (2001). On the change of support problem for spatio-temporal data. *Biostatistics*, 2(1):31–45.
- Gentemann, C. L. (2014). Three way validation of MODIS and AMSR-E sea surface temperatures. *Journal of Geophysical Research: Oceans*, 119(4):2583–2598.
- Gneiting, T. and Raftery, A. E. (2007). “Strictly proper scoring rules, prediction, and estimation”. *Journal of the American Statistical Association*, 102(477):359–378.
- Gotway, C. A. and Young, L. J. (2002). Combining incompatible spatial data. *Journal of the American Statistical Association*, 97(458):632–648.
- Guan, L. and Kawamura, H. (2003). SST Availabilities of Satellite Infrared and Microwave Measurements. *Journal of Oceanography*, 59(2):201–209.
- Haas, T. C. (1990). Kriging and automated variogram modeling within a moving window. *Atmospheric Environment. Part A. General Topics*, 24(7):1759–1769.
- Huang, H.-C., Cressie, N., and Gabrosek, J. (2002). Fast, resolution-consistent spatial prediction of global processes from satellite data. *Journal of Computational and Graphical Statistics*, 11(1):63–88.
- Kang, E. L., Cressie, N., and Shi, T. (2010). “Using temporal variability to improve spatial mapping with application to satellite data”. *Canadian Journal of Statistics*, 38(2):271–289.
- Katzfuss, M. and Cressie, N. (2011). “Spatio-temporal smoothing and EM estimation for massive remote-sensing data sets”. *Journal of Time Series Analysis*, 32(4):430–446.
- Katzfuss, M. and Cressie, N. (2012). “Bayesian hierarchical spatio-temporal smoothing for very large datasets”. *Environmetrics*, 23(1):94–107.

- Kawai, Y., Kawamura, H., Takahashi, S., Hosoda, K., Murakami, H., Kachi, M., and Guan, L. (2006). Satellite-based high-resolution global optimum interpolation sea surface temperature data. *Journal of Geophysical Research*, 111(C6):290–17.
- Lindgren, F., Rue, H., and Lindström, J. (2011). “An explicit link between Gaussian fields and Gaussian Markov random fields: the stochastic partial differential equation approach”. *Journal of the Royal Statistical Society: Series B (Statistical Methodology)*, 73(4):423–498.
- Ma, P. and Kang, E. L. (2018). A fused Gaussian process model for very large spatial data. *Journal of Computational and Graphical Statistics*. Under revision.
- Ma, P., Kang, E. L., Braverman, A., and Nguyen, H. (2018). Spatial statistical downscaling for constructing high-resolution nature runs in global observing system simulation experiments. *Technometrics*. To appear.
- Mardia, K. V., Goodall, C., Redfern, E. J., and Alonso, F. J. (1998). The kriged kalman filter. *Test*, 7(2):217–282.
- Marschner, I. C. (2001). On stochastic versions of the EM algorithm. *Biometrika*, 88(1):281–286.
- McMillan, N. J., Holland, D. M., Morara, M., and Feng, J. (2010). Combining numerical model output and particulate data using Bayesian space-time modeling. *Environmetrics*, 21(1):48–65.
- Nguyen, H., Cressie, N., and Braverman, A. (2012). “Spatial statistical data fusion for remote sensing applications”. *Journal of the American Statistical Association*, 107(499):1004–1018.
- Nguyen, H., Cressie, N., and Braverman, A. (2017). Multivariate spatial data fusion for very large remote sensing datasets. *Remote Sensing*, 9(2):142. DOI:10.3390/rs9020142.
- Nguyen, H., Katzfuss, M., Cressie, N., and Braverman, A. (2014). “Spatio-temporal data fusion for very large remote sensing datasets”. *Technometrics*, 56(2):174–185.
- Nielsen, S. F. (2000). The stochastic EM algorithm: Estimation and asymptotic results. *Bernoulli*, 6(3):457–489.
- Nychka, D., Bandyopadhyay, S., Hammerling, D., Lindgren, F., and Sain, S. (2015). “A multiresolution Gaussian process model for the analysis of large spatial datasets”. *Journal of Computational and Graphical Statistics*, 24(2):579–599.
- O’Carroll, A. G., Saunders, R. W., and Watts, J. G. (2006). The measurement of the sea surface temperature by satellites from 1991 to 2005. *Journal of Atmospheric and Oceanic Technology*, 23(11):1573–.
- Poole, D. and Raftery, A. E. (2000). Inference for deterministic simulation models: The Bayesian melding approach. *Journal of the American Statistical Association*, 95(452):1244–1255.
- Sahu, S. K., Gelfand, A. E., and Holland, D. M. (2010). Fusing point and areal level space-time data with application to wet deposition. *Journal of the Royal Statistical Society: Series C (Applied Statistics)*, 59(1):77–103.
- Shi, H. and Kang, E. L. (2017). Spatial data fusion for large non-Gaussian remote sensing datasets. *Stat*, 6(1):390–404.
- Stoffer, D. S. and Wall, K. D. (1991). Bootstrapping state-space models: Gaussian maximum

- likelihood estimation and the Kalman filter. *Journal of the American Statistical Association*, 86(416):1024–1033.
- Stroud, J. R., Müller, P., and Sansó, B. (2001). Dynamic models for spatiotemporal data. *Journal of the Royal Statistical Society: Series B (Statistical Methodology)*, 63(4):673–689.
- Vecchia, A. V. (1988). “Estimation and model identification for continuous spatial processes”. *Journal of the Royal Statistical Society: Series B (Statistical Methodology)*, 50(2):297–312.
- Wei, G. C. G. and Tanner, M. A. (1990). A Monte Carlo implementation of the EM algorithm and the poor man’s data augmentation algorithms. *Journal of the American Statistical Association*, 85(411):699–704.
- Wikle, C. K. and Berliner, L. M. (2005). Combining information across spatial scales. *Technometrics*, 47(1):80–91.
- Wikle, C. K., Berliner, L. M., and Cressie, N. (1998). Hierarchical Bayesian space-time models. *Environmental and Ecological Statistics*, 5(2):117–154.
- Wikle, C. K. and Cressie, N. (1999). A dimension-reduced approach to space-time Kalman filtering. *Biometrika*, 86(4):815–829.
- Wikle, C. K., Milliff, R. F., Nychka, D., and Berliner, L. M. (2001). Spatiotemporal Hierarchical Bayesian Modeling Tropical Ocean Surface Winds. *Journal of the American Statistical Association*, 96(454):382–397.
- Xu, K. and Wikle, C. K. (2007). Estimation of parameterized spatio-temporal dynamic models. *Journal of Statistical Planning and Inference*, 137(2):567–588.